ADVANCED BIOLOGY
www.advanced-bio.com

Rapid and Electronic Identification and Quantification of Age-Specific Circulating Exosomes via Biologically Activated Graphene Transistors

*Reza Hajian, Jonalyn DeCastro, Jonathan Parkinson, Alex Kane, Andres Felipe Romero Camelo, Peichi Peggy Chou, Jielin Yang, Nathan Wong, Ecson Daniel Obando Hernandez, Brett Goldsmith, Irina Conboy, and Kiana Aran**

Increasing access to modern clinical practices concomitantly extends lifespan, ironically revealing new classes of degenerative and inflammatory diseases of later years. Here, an electronic graphene field-effect transistor (gFET) is reported, termed EV-chip, for label-free, rapid identification and quantification of exosomes (EV) associated with aging through specific surface markers, CD63 and CD151. Studies suggest that blood-derived exosomes carry specific biomolecules that can be used toward diagnostic applications of age and health. However, to observe improvements in patient outcomes, earlier detection at the point-of-care (POC) is required. Unfortunately, conventional techniques and other electronic-based platforms for exosome sensing are burdensome and inept for the POC distinction of aged blood factors. It is shown that EV-chip can quantitatively detect purified exosomes from plasma, with a limit of detection (LOD) of 2×10^4 particles mL^{-1} and a limit of quantification (LOQ) of 6×10^4 particles mL^{-1}. The sensitivity and compact electronics of the EV-chip improves upon previously published electronic biosensors, making it ideal for a physician's office or a simple biological laboratory. The sensitivity, selectivity, and portability of the EV-chip demonstrate the potential of the biosensor as a powerful point-of-care diagnostic and prognostic tool for age-related diseases.

1. Introduction

Advances in access to public healthcare, modern clinical practices, and medical technologies have resulted in monumental achievement in extending the human lifespan. In an age where technologies such as smart wearables and devices intersect health and other aspects of biology,[1] there comes a natural evolution of disease diagnostics from its more conventional counterparts moving from central lab testing to point-of-care, digital health monitoring (**Figure 1**). Liquid biopsies offer the potential of more frequent sampling for health monitoring through biofluids such as saliva, urine, or blood and in the case of aging, early identification of age-associated disease biomarkers.[2] Many age-related disorders are discovered later in life,[3] where studies show that earlier diagnosis improve patient outcomes and satisfaction by providing the ability to change life habits or setting forth future life plans.[3–6] Although there are current liquid biopsy studies within the fields of healthy aging (the process at which lifespan is increased without the development of debilitating diseases)[7] and age-related diseases (ARDs), including degenerative diseases,[8] there appears to be a bottleneck in the discovery of aging biomarkers. This impediment is derived from the fact that most aging diagnostics occur with conventional tissue biopsies, within a central lab, with laborious procedures, and advanced equipment. All of these factors materialize into delayed diagnostics and clinical decision making at the point-of-care (POC) setting which is the stage where a patient is interacting with and seeking answers from their healthcare provider.[9,10] To

Dr. R. Hajian, J. DeCastro, A. F. R. Camelo, E. D. O. Hernandez, Dr. K. Aran
Keck Graduate Institute
The Claremont Colleges
Claremont, CA 91711, USA
E-mail: kiana_aran@kgi.edu

Dr. R. Hajian, Dr. J. Parkinson, Dr. A. Kane, Dr. B. Goldsmith, Dr. K. Aran
Cardea Bio Inc.
8969 Kenamar Dr. Suite 104
San Diego, CA 92121, USA

The ORCID identification number(s) for the author(s) of this article can be found under https://doi.org/10.1002/adbi.202000594.

DOI: 10.1002/adbi.202000594

P. P. Chou
Keck Science Department
Pitzer College
The Claremont Colleges
Claremont, CA 91711, USA

J. Yang
Keck Science Department
Claremont McKenna College
The Claremont Colleges
Claremont, CA 91711, USA

N. Wong, Dr. I. Conboy, Dr. K. Aran
Department of Bioengineering
University of California, Berkeley
Berkeley, CA 94720, USA

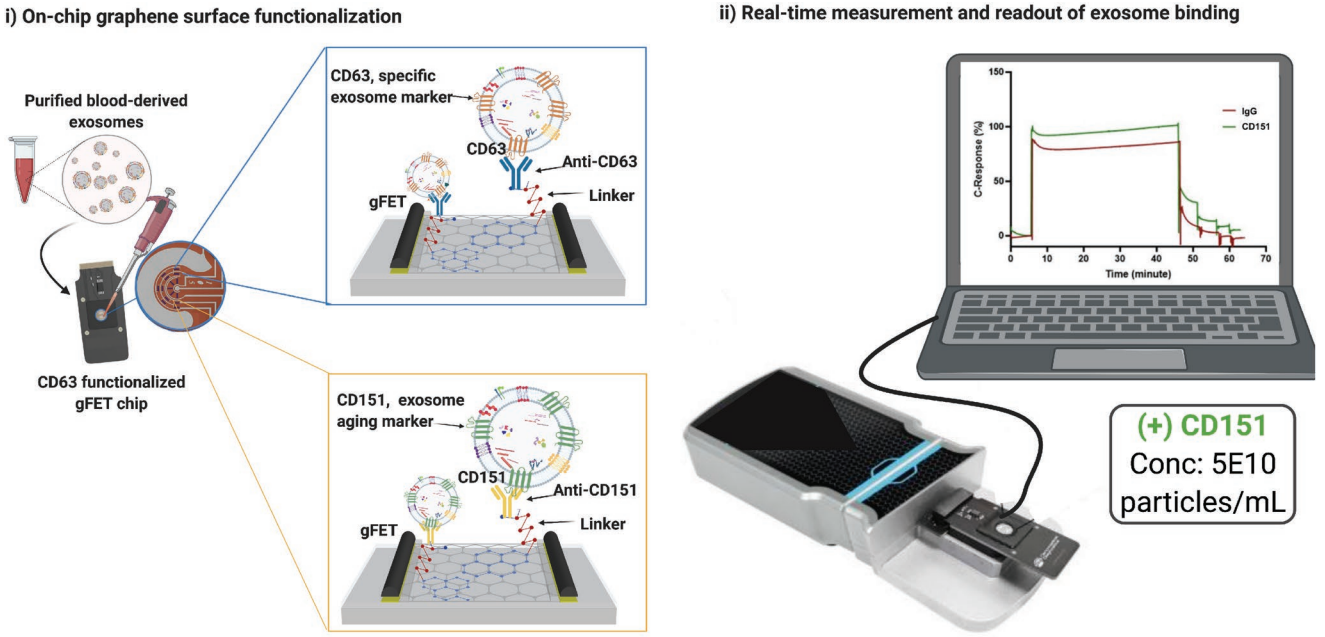

Figure 1. Schematic of Exo-Chip detection of blood derived exosomes from plasma samples. i) Anti-CD63 (top) or anti-CD151 (bottom) is functionalized onto the graphene monolayer with a chemical linker. Upon introduction of purified plasma-derived exosome samples to the graphene surface, CD63 exosome surface marker (top) is bound by anti-CD63 introducing a change in electrical properties detected by the gFET sensor. CD151 exosome surface marker (bottom) is bound by anti-CD151 in a similar fashion. ii) Real-time measurement and electrical readout of EV-Chip detection of general and age-specific exosomes with correlation to concentration of exosomes in particles/mL. Created with BioRender.com.

transition age-related diagnostics to the POC, testing for the aging biomarkers must be within the sensitivity and specificity of the central lab. Additionally, it requires that samples are robust, stable, and minimally processed while results are rapid and easy to interpret for clinical and biomedical professionals.[10–13] Furthermore, aside from monitoring disease associated aging, there is a similar urgency to establish a means of monitoring healthy aging as a way of predicting the trajectory of ARDs onset in a population and longitudinally.

Interestingly, a group of biomarkers with growing influence on age-related liquid biopsies include extracellular vesicles, particles that are shed by most, if not all, cells.[14] Recently exosomes (EVs), the smallest of extracellular vesicles ranging from 30 to 150 nm in diameter, have been implicated in intercellular communication across tissues and cell lines among aging and other biological pathways through their surface and encapsulated proteins and nucleotides (DNA and RNA).[7,15–20] Exosomes follow an endosomal pathway for synthesis which includes the multivesicular body (MVB) and endosomal sorting complex required for transport (ESCRT) pathways. Due to these sorting pathways, an exosomes' vesicle formation allows it to carry both information regarding parent cell organelles and plasma membrane characteristics.[21–23] Some common exosome surface markers that differentiate them from larger vesicles include the tetraspanins, CD63, CD81, and CD9. A tetraspanin exerts its role through interactions with integrin-mediated cell adhesion with major roles in the late endosomal and MVB pathway of releasing vesicles.[24] More specifically CD63, which is a surface protein of exosomes, is involved in many other cell-migration and cell-adhesion events. For example, CD63 co-localization with Syntenin-1[25] or L6-antigen[26] in many types of cancers or trafficking of CD63 to chemokine receptors for viral infection of immune cells.[27–30] Due to these interactions, many other tetraspanins and exosome surface markers are prime candidates for disease biomarkers including those for age-associated diseases.[30]Recent studies comparing conventional immunoassays and antibody arrays studied age-related effects of purified plasma exosomes and found a panel of markers that varied between young and old human blood samples.[7,31,32] Of note, the tetraspanin CD151, typically associated as a cancer biomarker with prognostic and diagnostic value in tumor metastasis[33] was found to be associated with healthy aging in both Eitan et al. longitudinal and cross-sectional studies of two visits spanning a five-year difference.[7] Exosome analysis observed CD151 to be increased in expression from young to old populations in both aging studies. Furthermore, CD151 as a tetraspanin, surface receptor on exosomes exerts its role similar to CD63 in cell-adhesion and cell motility events potentially giving insight on some cancer invasion mechanisms.[7,34] It was suggested that the age-associated increase in CD151 protein levels on the exosome's surface could be further investigated as a clinical age biomarker given additional studies.[7]

Conventional techniques for analyzing exosome liquid biopsy samples include mass spectrometry or immunoassays similar to those in Eitan et al. These techniques require larger sample volumes, overnight incubation, or optical labeling. Furthermore, nucleic acid assays such as RT-qPCR or next generation sequencing require advanced expertise and time.[35–37] These assay requirements subsequently demand equipment not amenable for routine monitoring at point-of-care. Therefore, label-free miniaturized electronic biosensing platforms have significant interest given they allow for longitudinal moni-

toring of a patient's health state from minute starting samples[38] making point-of-care liquid biopsies a possibility. Recent studies on the optimization of exosome detection within liquid biopsies include ways to integrate continual measurements of varying analytes with different materials in a biosensor such as detection with aptamer-coated surfaces or coating a metallic surface with chemical linkers.[39] Additionally, graphene-based field-effect transistors (gFETs) have been employed for exosome detection through the use of antibody-antigen interactions.[40] However, constraints of this previously published electronic based system for exosome detection are that they are difficult to use, expensive, and bulky. Moreover, this system is typically found within an electronics lab with electrical results that may even require a high degree of engineering expertise in order to interpret.[40]

Here, we report an exosome specific gFET termed EV-chip that combines the high electrophoretic mobility of exosomes, the specificity of antigen–antibody interaction between exosome specific bioreceptors with the sensitive detection of a gFET for real-time digital feedback on exosome analyte quantification. Moreover, the EV-chip reader is designed as a prototype portable, low-cost reader. The electrical components of the reader are cost-effective and affordable, where the entirety of the unit weighs less than 5 kg and is about the size of a large smart phone. The reader consists of a picoammeter, potentiostat, multiplexer, analog to digital converter, digital to analog converter, microprocessor controller, and serial interface. The entire system is constructed via standard PCB manufacturing processes; there are no patch cables or hand soldered connections; it is a true proof of concept for an integrated system. Custom firmware has been written to drive this reader and the reader subsequently connects easily to any computer via USB. The capabilities of this reader to simplify software communication while combining control circuits, various voltage driving circuits, and measurement circuits onto one board represents a significant step toward moving graphene chip based biosensing out of the electronics laboratory environment. Collectively, EV-chip has simplicity in instrumentation and portability as a hand-held electronic biosensor that would fit the needs of a small biomedical science laboratory or physician's office. (Figure 1). Briefly, the gFET is constructed with three terminal electrodes (source, drain, and gate) and the output signal is modulated by the gate electrode, consisting of the sample liquid and a layer of functionalized bioreceptors which also serve as the gate dielectric. The power of the EV-chip system is due to the combination of specific interaction of exosome tetraspanin biomarkers with corresponding antibodies and the graphene. Graphene has a high carrier mobility (>2000 $cm^2V\ s^{-1}$),[39–41] making it sensitive to adsorption and interaction of charged molecules at its surface. This is ideal for exosome detection given their zeta-potential of between −30 to up to −50 mV in certain buffer conditions; where the zeta-potential is the potential difference between the surface charge of a particle immersed in a conductive liquid.[42] Different parameters between the source, drain, and gate can be monitored through each transistor, which allows for quantitative measurement of exosome tetraspanins, all recorded in real-time and within less time and required volumes than conventional immunoassays, with the ease and convenience of a "USB-like" plug-in assay chip.[43] This gFET platform is modifiable for different analyte detection and has already proven its ability of acute detection of specific proteins and gene sequences in previously developed platform variants.[44,45] In this study we explore a superior gFET for detection and quantification of age-specific biomarkers on the surface of purified plasma-derived exosomes that is more appropriate for a biological lab or POC setting.

2. Results and Discussion

2.1. Characterization of Purified Exosomes

The purified exosomes isolated by size-exclusion chromatography were collected as five-5 mL fractions and the fractions with the smallest diameter, ideal for exosome sensing within the Debye length (Figure S1 Supporting Information), were used for downstream analysis. Fractions 1–5 for all three young and old donors were positive for exosome-like diameters. However, fractions 4–5 for the young and old donor samples appeared to be the smallest size diameter particles and were used for characterization and EV-chip analysis. Exosome fractions 4–5 were characterized with nanoparticle tracking analysis (NTA) for exosome-like size and concentration, Bradford assay for total protein concentration, scanning electron microscopy (SEM) for vesicular shape, and ELISA for CD63-expression specific to exosomes. A comparison of young and old exosome characteristics was found to show no significant difference between particle concentration, total protein concentration, or specific CD63 concentration between young and old (**Figure 2**) (Welch's *t*-test, $p > 0.05$, $N > 2$).

A representative graph of purified exosomes used for characterization shows a median diameter of 98 nm (Figure 2A), with sample concentration of 1.2×10^{10} particles mL^{-1}, as measured by NTA. Under the dynamic flow conditions of NTA analysis, particle events are tracked through video recordings and logged based on path trajectory (Figure 2A inset). In a comparison of the young and old plasma donors and the exosome concentrations of fractions 4–5, no significant difference was found between young and old exosome concentrations (Figure 2B, left and right) ($p > 0.05$; two-tailed *t*-test). Additionally, comparison of old and young exosomal, total protein concentration yielded similar results (Figure 2C) ($p > 0.05$; two-tailed *t*-test).

To evaluate the effectiveness of exosome capture on EV-chip through binding with CD63 antibody, we exposed the anti-CD63 immobilized chip to a solution containing suspended exosomes at a concentration of 5×10^9 particles mL^{-1} in 1 × PBS. After immobilization at 37 °C for 40 min and sequential rinsing with 1/1000 × PBS, the surface of gFETs was then characterized by SEM.[46–48] SEM was also implemented on pristine graphene for a comparative examination of exosome-altered surface morphology. Displayed in Figure 2D, the SEM image of pristine graphene reveals regions of various carrier densities due to different layers of graphene and of note, an absence of exosomes along the pristine surface. In contrast, Figure 2E shows the distribution of captured exosomes on the antibody-functionalized surface with the size distribution of about 56–120 nm. These gFETs-binding nanoparticles can be well validated as exosomes since their sizes are distinguishable from other cell-derived vesicles.[14,42]

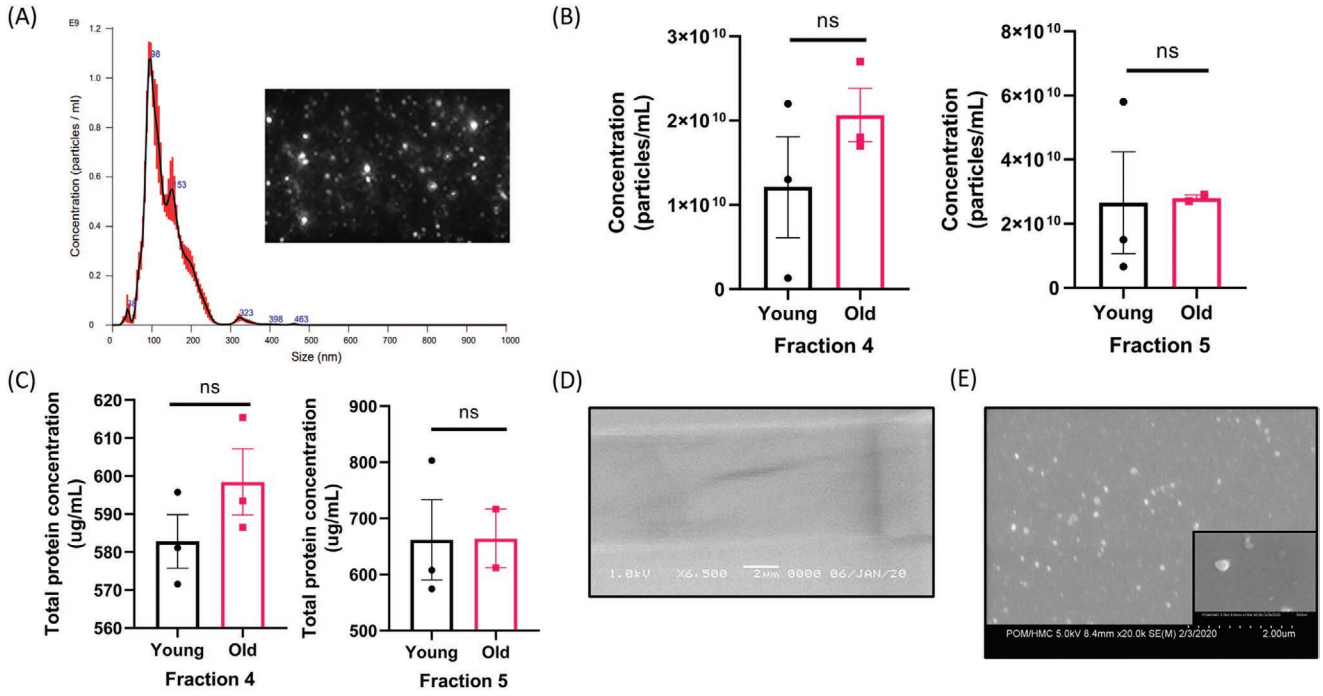

Figure 2. Characterization and validation of exosome samples. A) Size and concentration distribution of purified exosomes by nanoparticle tracking analysis (NTA). Inset: Tracking of exosomes particles by NTA software to derive the particle size distribution. B) Comparison of NTA validated concentrations of Fraction 4 (Left) and Fraction 5 (Right) isolated from size-exclusion column (SEC). C) Comparison of total protein concentration from Bradford assay at A595 of Fraction 4 (Left) and Fraction 5 (Right) isolated from SEC. NS for this and all other subplots indicates the difference in means is not significant (Welch's *t*-test, $p > 0.05$, $N = 3$ for Fraction 4 Y, O and Fraction 5 Y. $N = 2$ for Fraction 5 O. D) Scanning electron microscopy of pristine graphene. E) Exosomes bound on anti CD63. E) Inset: Exosomes particles on functionalized chip with anti-CD63 at high magnification.

2.2. Exosome Detection by EV-Chip

The initial electrical characteristics of EV-chip for each functionalization step was performed by transfer curve measurements (**Figure 3**A) as a function of source-drain current (I_{SD}) versus gate voltage (V_G) for monitoring each stage of exosome sensing from a pristine graphene surface, through surface functionalization, and exosome detection. The device characteristics of pristine graphene show the typical ambipolar transport behavior with a minimum I_{SD} at 0.734 V, which conforms to the charge neutrality point (the Dirac point) in graphene. The gate dependence of source-drain current reveals an evident change upon the functionalization of graphene with the linker (1-pyrenebutyric acid, PBA) as the Dirac point shifts to 0.639 V. This change corresponds to n-type doping on graphene by PBA. Furthermore, covalent immobilization of CD63 antibody on EV-chip has a negative shift of Dirac voltage (0.581V). This is due to the n-type doping of the negatively charged antibody. The observed change of the conductivity, as manifested in the transfer curves, can be attributed to a variation in the resistance of graphene during its interaction with the immobilized antibody. Illustrated in Figure 3A, the gate dependence of source-drain current has a significant shift in Dirac voltage to 0.523 V in the range from 0.0 to 0.8 V after immobilization of exosomes on the captured antibody. The change in slope corresponds to the change in capacitance inside the Debye layer between the graphene channel and gate. Thereafter, for actual measurements and to transition from heavy instrumentation to our finalized hand-held reader device, the real time data as function of current and capacitance versus time was monitored for the detection of plasma purified exosomes.

The capacity of EV-chip for real-time measurement of exosome binding was demonstrated by synchronous data collection (Agile, Cardea Bio, USA). The gate voltage sweeps in a limited range of ±0.1 V with a frequency of 3.3 Hz at a fixed source-drain voltage of –0.05 V. The slope of the transfer curve was measured, and data was plotted against time. To substantiate the specificity of exosome–antibody interactions, we functionalized the surface of gFET with two different antibodies (monoclonal antibodies against human CD63 and human IgG1 isotype as the control). Anti-CD63 and IgG1 were immobilized on two singleplex chips by using PBA. They were activated via carbodiimide chemistry and were passivated with BSA to minimize non-specific interactions. Finally, the functionalized chips were calibrated with 1/1000× PBS, and the binding of the plasma purified – exosomes on two different immobilized antibodies was measured in real-time (Figure 3B). In order to control the Debye layer screen effect[38,39] and to enhance the sensitivity of detection, 1/1000× PBS was used as the assay buffer (Figure S1, Supporting Information). Timing for each of the liquid exchange steps is described in Experimental Section. All stepwise exchanges proceeded via an aspirator and manual pipetting. Aspiration of liquid from the sensor surface briefly removes the liquid gate before re-establishing it with a new sample on the surface. Such a procedure leads to the spikes in the data at the junctions.

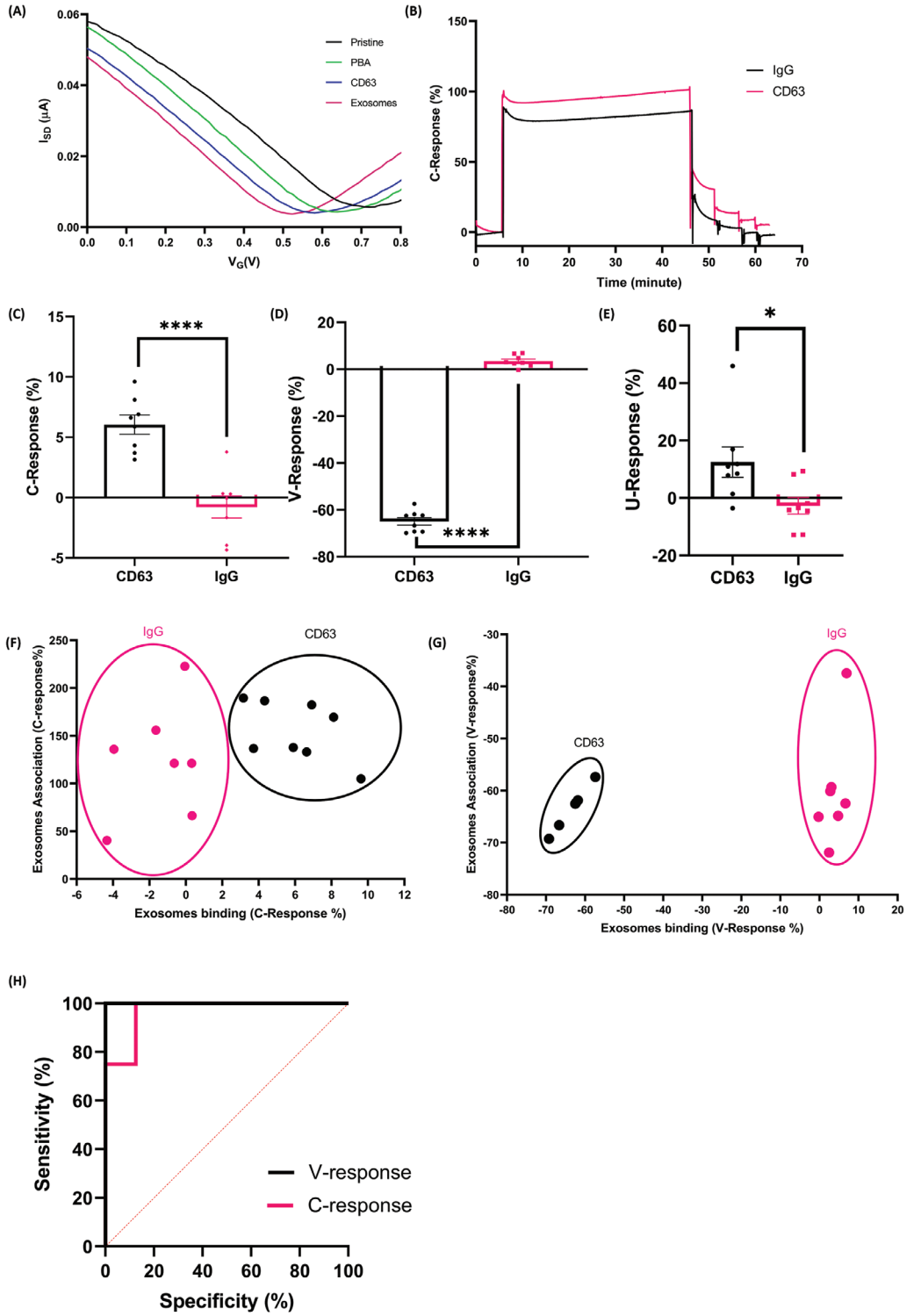

Figure 3. Exosome detection of EV-chip through CD63 on-chip binding. A) Transfer curves of gFET in the gate voltage range of –0 to 0.8 V for pristine graphene channel, after 1-pyrenebutyric acid (PBA) linker functionalization, CD63 antibody and exosomes. B) Real time response of EV-chip during calibration, exosomes immobilization (5×10^9 particles mL^{-1}) and subsequent rinsing with washing buffer for CD63 and IgG1 (control) functionalized chips. The EV-chip responses in terms of C-response. C) C-response by chip functionalization type (anti-CD63, anti-IgG) for human plasma exosomes for the EV-chip; $p < 0.0001$ (Welch's *t*-test, two-tailed; $N = 8$). D) V-response for the same; $p = 0.0002$ (Welch's *t*-test, two-tailed; $N = 8$). E) U-response for the same; $p = 0.02$ (Welch's *t*-test, two-tailed; $N = 8$). F) 2D graph of exosomes association C-response and V-response ($N = 15$) G) at the end of exosomes loading on the chips immobilized with anti-CD63 and IgG versus C-response at the end of exosomes dissociation by 1/1000× phosphate buffer saline (PBS) ($N = 14$). H) AUC-ROC for separation by experiment type and response type ($N = 16$) (*, **, ***, **** and ns, respectively, indicate $p < 0.05$, $p < 0.01$, $p < 0.001$, $p < 0.0001$ and $p > 0.05$ using a two-tailed Welch's *t*-test for relevant subplots.)

Molecular interactions at the surface of graphene create local potentials that effectively gate and alter gFET's electrical characteristics, including conductance, source-drain current (I-Response), the capacitance between the gate electrode and graphene channel (C-Response), surface potential of the graphene itself (V-Response), and the change in curvatures of the transfer curves (U-Response). As a result, the interaction of exosomes with immobilized antibodies is measurable as a change in one or more of these gFET properties, which can be measured simultaneously and in real-time. As Figure 3C elucidates, there is a significant change in C-response between two EV-chips after incubation with exosomes on the CD63 antibody immobilized chip versus the IgG1 antibody immobilized chip. The C-response (%) for exosomes on anti-CD63 is higher than the of IgG1 because exosomes (CD63 expressed) accumulate more intensively on the chip due to specific interaction with CD63 antibodies. Figure 3C shows the average C-response of EV-chip ($n = 8$) documented by the reader on anti-CD63 and IgG1-immobilized antibodies, respectively. These data were extracted at the end of the rinsing steps with 1/1000× PBS after subtraction from calibration. We observed a significant difference ($p<0.0001$, two-tailed *t*-test) between the two sets of data, indicating specific binding of CD63 exosomal protein with CD63 antibodies on gFETs. Moreover, data analysis shows that the surface potential (V-response, %) alters significantly ($p<0.0001$, two-tailed *t*-test) for exosomes bound on anti-CD63 in comparison with the control IgG1 antibody (Figure 3D). Similarly, Figure 3E illustrates that the value of U-response significantly alters based on the surface antibodies for human exosomes as another property of the gFET biosensor ($p<0.02$, two-tailed *t*-test).

Cluster analysis, also known as clustering, is the analysis by classifying a set of subjects in such a way that subjects in the same group (called a cluster) are more similar to each other than to those in other groups.[49] Figure 3F shows two clusters based on the distribution of data in exosomes incubation response (C-response, %) versus exosomes binding to CD63 or IgG1 surface antibodies in the last step of rinsing. The cluster analysis on V-response also reveals two distinguished groups in accordance with response measurement in the last step of rinsing with 1/1000× PBS (Figure 3G). While distinct separation in Y-axis (C-response and V-response) is not observed during exosomes incubation with CD63 and IgG1 immobilized antibodies, the clustering is mostly based on exosomes binding on antibodies after post-incubation and rinsing off non-specific bindings on graphene surface with 1/1000× PBS. V-response provides better separation between groups as illustrated by Figure 3H; the AUC-ROC and distance between group means is improved.

2.3. Real-Time Quantification of Exosomes, Calibration Curve, and Sensitivity

Unlike some commonly used methods for quantification of exosomes and surface biomarkers that require the use of secondary labels for optical quantification, EV-chip is a label-free biosensor with the capacity of real-time monitoring. Labeling-based detection is a time-consuming and cost-ineffective process.[43,49] However, EV-chip resolves these issues based on its short analysis duration in real-time and electrical, label-free detection. As shown in **Figure 4**A, the amplitude of C-Response increases logarithmically in parallel with increasing exosomes concentration during the first 5 min after incubation on the chip. The calibration Equation (1) fits in a logarithmic model as:

$$\begin{aligned} &\mathrm{C-response}\,(\%) = 0.1(\pm 0.01)\log C + 0.5(\pm 0.05) \\ &C : \text{concentration of exosomes}\left(\text{particles mL}^{-1}\right) \end{aligned} \tag{1}$$

The limit of detection (LOD) was calculated as 2×10^4 particles mL^{-1} based on $3.3S_b/m$, where S_b, is the standard deviation of the intercept in the calibration curve, and m is the sensitivity (slope of calibration curve).[50] Similarly, the limit of quantification (LOQ) was reported as 6×10^4 particles mL^{-1} based on $10S_b/m$.[49,50]

The EV-chip exhibits higher sensitivity, more comprehensive calibration range, and shorter response time (5 min) for exosomes detection in comparison with ExoELISA-Ultra CD63, a common commercially available exosome quantification kit. Figure 4B reveals the ExoELISA calibration curve (1.4×10^9–2.2×10^{10} particles mL^{-1}) for human plasma-purified exosomes, indicating a high concentration prerequisite for a valid analysis, concomitantly requiring a 5-h assay time. Overall, EV-chip with the equipped gFET technology is the faster and the more sensitive alternative for exosome quantification and validation. Moreover, it is a portable biosensor that can connect the Agile reader (Cardea Bio, USA) for real-time and point-of-care detections.

In addition, EV-chip reproducibility was studied by measuring the relative standard deviation (RSD) or the coefficient of variation for a sample (CV) obtained from EV-chip-functionalized with CD63 and IgG from 30 sensor devices after incubation with 10^9 particles mL^{-1} of human healthy plasma exosomes. The results, shown in Figure 4C, indicate an average C-response of −3.98 and 2.45 for CD63 and the control (IgG) surface biomarkers with RSDs of 1.37 and 1.07, respectively, which shows good reproducibility and specificity of EV-chip in detection of exosomes. Reproducible statistics was defined based on a RSD or CV < 20% based on quantitative ligand binding assay requirements set in both the laboratory[51] and industry guidelines.[52]

2.4. Preclinical Diagnostic Capacity of EV-Chip for Aging Biomarkers

Encouraged by our results on EV-chip as a label-free and real-time biosensor with improved sensitivity and specificity than those of a commercially available exosome ELISA (ExoELISA-Ultra CD63), we further assessed EV-chip for capacity to measure the biomarkers of aging. One such biomarker is CD151, a member of the tetraspanin superfamily which plays a critical role in regulation of cell signaling networks, migration, and metastasis, where the level of CD151 expression was found to be associated with cancer and aging.[7,33] Therefore, we obtained human plasma samples of both young ($n = 3$) and old ($n = 3$) subjects with no known hematopathy to control for confounding variables that may affect the level of CD151

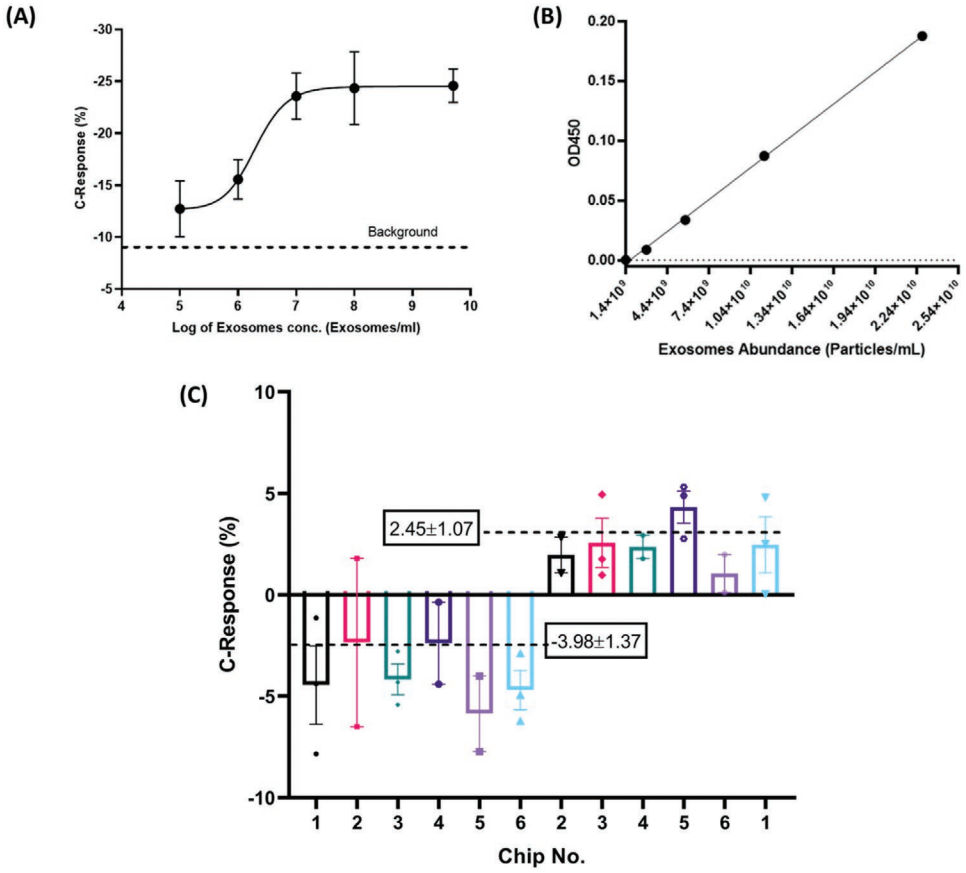

Figure 4. A) Calibration curve of EV-chip in the concentration range of 10^5 to 5×10^9 particles mL^{-1} using anti-CD63 as the capture antibody, fit to a four-parameter logistic. C-response (%) was measured after signal subtraction from the first calibration step in 1/1000× phosphate buffer saline (PBS). The mean and standard error of the mean (SEM) at each concentration is shown. ($N > 5$ for each concentration) B) Standard curve of ExoELISA-Ultra CD63 Kit for human purified plasma exosomes in the range of 1.4×10^9 to 2.3×10^{10} particles mL^{-1} ($N = 2$ for each concentration). C) Reproducibility of individual EV-chips functionalized with CD63 and IgG in the presence of 5×10^9 particles mL^{-1} human healthy plasma exosomes ($N = 30$).

expression in exosomes. Both young and old samples underwent similar exosome extraction and validation studies as previously described (Figure 2) to assess distinguishable differences in innate exosome characteristics regarding age. No significant differences were found in exosome diameter size range, total protein concentration, or specific exosome protein concentration of surface marker CD63 between old and young samples (Figure 2). These preclinical human plasma purified exosomes were used for downstream CD151 aging analysis on EV-chip.

Figure 5A,B represents a preliminary control experiment, where significant differences in C-response can be observed between exosome binding on immobilized CD63 and IgG1 isotype antibodies (average $p < 0.0001$, two-tailed *t*-test). The distinctions in C-responses, which indicate specific interactions between exosomes and CD63 antibodies, confirm not only the specificity of EV-chip's detection capacity but also the homogeneity of biomarker expression across young human plasma samples. Similarly, the same procedure was repeated for the three old human plasma samples, and the results validate their homogenous nature as well (Figure 5C,D).

To evaluate if EV-chip could distinguish sample differentiation with specific biomarkers, CD63 and CD151 antibodies were functionalized on two chips with PBA, respectively, for each individual human plasma sample. Figure 5E elucidates the average C-response for both young and old exosome samples against CD63 immobilized antibodies. No significant difference was found, and the results were further confirmed with ExoELISA CD63 (Figure 5F) as the level of exosomes expressing CD63 remains consistent across ages ($p > 0.05$, two-tailed *t*-test). However, as it has illustrated in Figure 5G, exosome binding on anti-CD151 immobilized chips is manifested by significant difference in C-response levels between each pair of young versus old human plasma samples ($p < 0.001$, $p < 0.05$, $p < 0.001$, two-tailed *t*-test). Although some variations exist across each pair of donors, the average response levels detected by EV-chip (Figure 5H) shows a distinct separation of C-responses (approximately 7%) between young and old samples ($p < 0.001$, two-tailed t-test). Upon further analysis of old and young cohorts, Python Scikit-learn was used to perform mean-imputation and normalization on the C-responses. Python sciPy was subsequently used to approximate old and young cohorts to a univariate normal distribution and the linear discriminant analysis (LDA) boundary was computed by subtracting the resulting probability density functions. Figure 5I follows recent findings in literature that CD63 is a general marker for exosomes (e.g., not age-related).[7,14] This figure shows the overlap between the

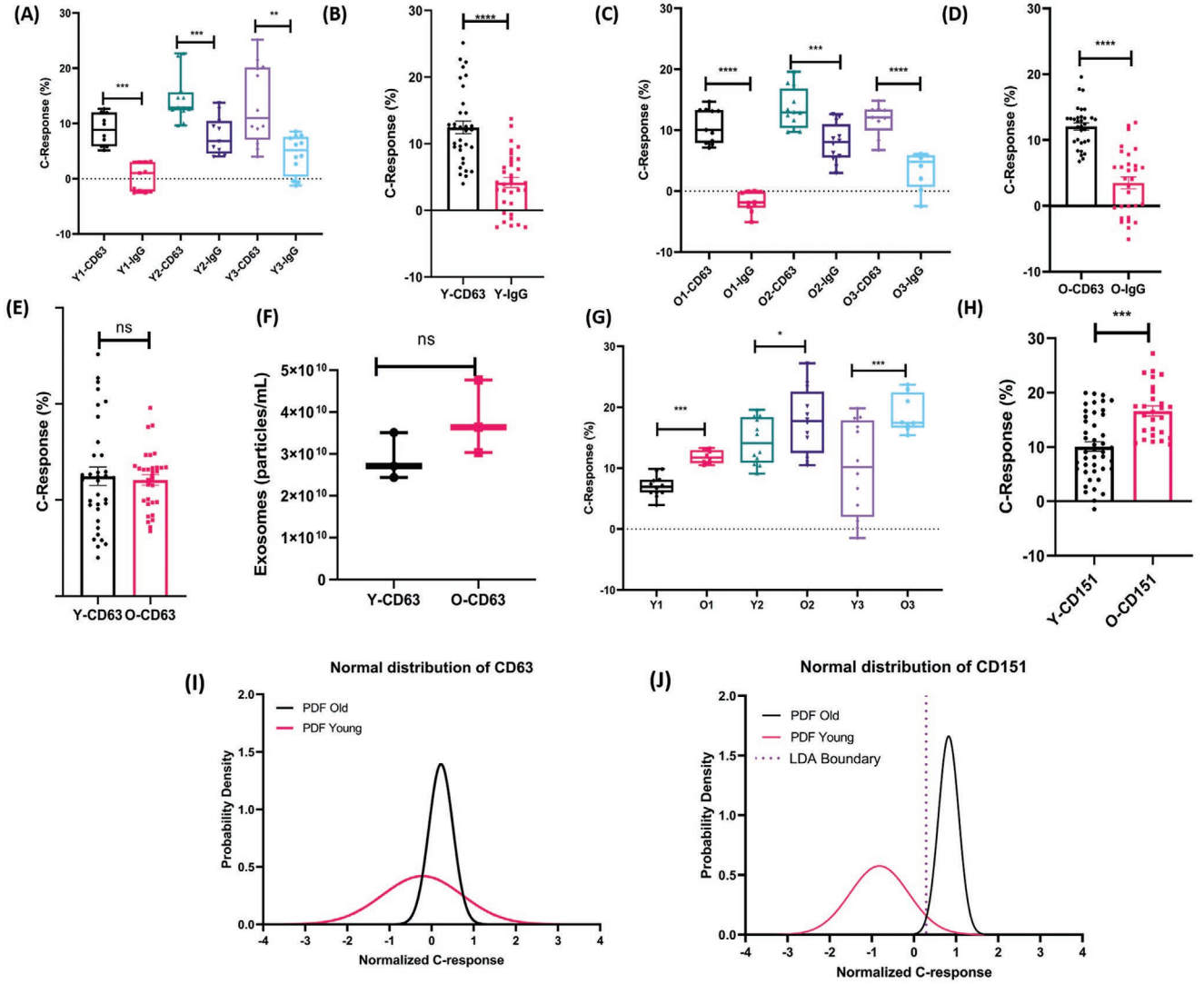

Figure 5. Pre-clinical detection capacity of EV-chip for aging biomarkers. A) The C-response of EV-chip for individual young ages human plasma donors against CD63 and IgG1 (control) antibodies. *, **, ***, **** and ns, respectively, indicate $p < 0.05$, $p < 0.01$, $p < 0.001$, $p < 0.0001$, and $p > 0.05$ using a two-tailed Welch's *t*-test for this and all other subplots ($N > 10$ for all conditions). B) The average responses of three young donors against CD63 and IgG1 (control) antibodies ($p < 0.0001$) ($N > 30$ for all conditions). C) The C-response of EV-chip for individual old ages human plasma donors against CD63 and IgG1 (control) antibodies ($N > 8$ for all conditions). D) The average responses of three old donors against CD63 and IgG1 (control) antibodies ($p < 0.0001$) ($N > 30$ for all conditions). E) The level of CD63 biomarker between young and old plasma ages is not significant ($p = 0.8977$) ($N > 30$ for all conditions) and F) validated with ELISA ($p > 0.05$) ($N = 3$). G) The C-response of EV-chip for individual young and old plasma exosomes against CD151 aging biomarker ($N > 8$ for all conditions). H) The average response of EV-chip for three old and three young donors against CD151 aging biomarker ($p = 0.0002$) ($N > 27$ for all conditions). I) The univariate normal probability density function of CD63 C-response was estimated for old and young cohorts. J) The univariate normal probability density function of CD151 C-response was estimated for old and young cohorts. The linear discriminant analysis (LDA) boundary was also computed to display the separation between old and young cohorts based on CD151.

two probability density distributions of old and young samples, which confirm studies showing that CD63 is not differentially expressed with age. Although in Figure 5J, the univariate normal probability density function of CD151 C-response was estimated for old and young cohorts. The LDA boundary was also computed to display the separation between old and young cohorts based on CD151. This figure shows that CD151 is differentially expressed with age. We have shown that Exo-chip is able to faithfully detect age-related association in binding, which is broadly applicable to numerous biomedical applications.

Due to the consistent gFET functionalization (anti-CD151) and an observed steady CD63 level across age, bindings with both young and old plasma exosomes are specific, and the differences in exosome detection rate can only be attributed to an elevation of CD151 expression in parallel with age. This result confirms the association of CD151 with age as expected.[7] Therefore, EV-chip displays its prowess as an exosome detection device with potential applications in clinical diagnosis, namely the capacity to quickly and sensitively assay exosomal surface biomarkers that are age and disease specific. In conjunction

with its real-time and label free characteristics as well as its portable nature, easy application on various ARDs diagnosis can be possible with plasma-derived exosomes.

3. Conclusion

In the present study, we developed EV-chips with monolayer gFETs and chemically functionalized them for real-time detection of exosomes with enhanced sensitivity, specificity, and clinical feasibility. Efficacious doping of chemical linkers with a high concentration of PBA on pristine graphene and the immobilization of antibodies are supported by the alternations of Dirac point as well as the change in the slope of the transfer curve for each step during functionalization. As a result, human plasma- purified exosomes can be quantified at ultrasensitivity with a limit of detection (LOD) as low as 8×10^4 particles mL^{-1}, which upon comparison to commercially available ELISA kits used within a central lab amounts to an improvement of sensitivity on the order of 10^4–10^5 times more sensitive – a notable improvement over most existing methods.[43,53–56]

We believe that this increased sensitivity is partially due to the migration of exosomes toward the positive, p-doped graphene surface. Exosomes in 1×10^{-3} M PBS buffer exhibit a −30 mV zeta-potential in pH 6.9,[42] whereas exosomes in 0.01×10^{-3} M PBS buffer were observed to have zeta-potentials downwards of −50 mV. Additionally, it is suggested that with less ionic strength of the buffer, there is less counterion screening of the exosome's natural colloidal suspension,[42] so a buffer with even less ionic strength could yield a much more negative zeta-potential. Given that we used a 1/3× PBS buffer for exosome binding upon the graphene monolayer and using 1/1000× PBS as the rinsing buffer during exosome detection, it is assumed that due to the highly negative zeta-potential of exosomes, the exosomes are electrostatically attracted to the positively charged graphene. As the exosomes come into proximity with the graphene, another highly favorable phenomenon occurs: the event of a thermodynamically favorable antibody to antigen binding. In general, antibody and antigen binding has a negative Gibbs free energy (ΔG) which allows the reaction to occur spontaneously without the addition of external energy.[57–60] In the case with EV-chip, there is anti-CD63 or anti-CD151 interaction with their respective antigens on the surface of exosomes (CD63 or CD151 tetraspanins) within the Debye length which further contributes to exosome interaction and detection on the graphene surface.

Time-varying electrical characteristics on the surface of the graphene, reflect real-time molecular interactions, predominantly, exosome association and binding which are measured in various forms. EV-chip has the capacity to differentiate specific biomarkers on the exosomes, elucidated by distinct C, V, and U-responses between anti-CD63-immobilized gFET sensors and its isotype, IgG1. Higher responses for exosome binding, instead of association, suggest a precise and exclusive interface populated with CD63 expressed exosomes.

The potential utilization of the sensor for comparative detection of CD151 positive exosomes in the young and old adults is interesting as a way to monitor the process of aging. Furthermore, it entails applications for longitudinal life-span studies, as well as an early detection of age-related diseases. Equally compelling is the use of the gFET exosome sensor for studying the role of CD151 in intercellular communication.[33] Due to this nature as a tetraspanin, CD151 is known for its effects on tumor progression, functioning as a regulator of post-adhesion events such as cell migration, spreading and invasion.[7,33,61] In this regard, it is notable that age is one of the major risk factors of cancer, and CD151 increases with age in blood might be measurable with the EV-chip.

Our studies indicate the potential of EV-chip for label-free, rapid electronic identification and quantification of circulating exosomes which has the potential to be used for early assessment of biomarkers of aging and disease. Future studies of larger pre-clinical cohorts may help strengthen this notion and solidify EV-chip as a valuable diagnostic tool. Compared to conventional assays that may require overnight incubation,[43,54–56,62] EV-chip's specific exosome detection takes place within 1 h. This time frame fits well within the bounds of a normal physician's visit, making EV-chip convenient and applicable for discriminating between aged blood factors within a standard clinical setting. By altering the antibodies immobilized on the gFETs, EV-chip has the flexibility for quantification and validation of various biomarkers for easy diagnosis and prognosis of common ARDs such as cancer, cardiovascular disease, and neurodegenerative disorders.[31,63,64]

Moreover, the measurement approach and system we have designed for the EV-chip is appropriate for use in a simple, biology laboratory or POC under the supervision of a biomedical professional, and without any specialized training.[40] In addition, the EV-chips are designed and packaged such that they can be easily swapped in and out of the measurement system quickly, like the way one would plug in and out a USB connection. As a result, the measurement throughput is significantly larger than what is seen with other graphene sensor chips or electrical biosensors.[40] Equally important is the fact that the EV-chip is single use, making it ideal for a clinical setting, where any sort of diagnostic or monitoring using exosomes would require exposure to biofluids such as blood or serum. This reduces the demand of sterilization within the POC setting.

Furthermore, complex biofluids, such as blood, carry multiple biomarkers including external or internal cargo of exosomes. EV-chip can be readily reconfigured for detection of these different biomarkers individually or in combinations, expanding the detection of one biomarker to a panel utilizing a highly multiplexed platform. Studies suggest that gFETs may be employed for multiparametric analysis, which demonstrates the potential of EV-chip as a multiplexed analysis tool for simultaneous monitoring of exosome multiomics from minute sample volumes while covering a myriad of age-associated diseases. The design of the EV-chip and chip reader allows for convenient adaptability from its original design featured here to one that incorporates a large number of transistors within a single compact chip. Within this multiplexed, EV-chip design, detection of numerous exosome biomarkers can occur rapidly and simultaneously while still being controlled and analyzed using a single chip reader. Additionally, the electronic nature of EV-chip allows for high quality and digitized electronic measurements that are inherently compatible with machine learning techniques

capable of reconfigurability from hand-held to bench top systems. Uniquely as well, EV-chip can be multiplexed for application in sorting of exosomes from different cells, given that there are issues of heterogeneity in plasma-derived exosomes for clinical applications.[65] In short, EV-chip, with its embedded gFET technology can be used as an effective, label-free digital liquid biopsy tool to harness the diagnostics value of exosomal biomarkers for aging and age-related diseases.

4. Experimental Section

Antibodies for EV-Chip Detection of Exosomes: Human CD63 antibody (R&D systems, USA) was reconstituted at 500 mg mL^{-1} in sterile 1× PBS. Human IgG1 Isotype (ThermoFisher, USA) was reconstituted at 100 mg mL^{-1} in sterile 1× PBS. Human CD151 antibody (R&D systems, USA) was reconstituted at 500 mg mL^{-1} in sterile 1× PBS. All the resuspended antibodies (human CD63, human IgG, and human CD151) were kept at –20 °C in small aliquots before using on the EV-chip. Bovine serum albumin (Sigma Aldrich) was made at 5 mg mL^{-1} in 1× PBS and it was kept at –20 °C in small aliquots.

Exosome Purification: For initial EV-chip validation studies, pooled Human Complement Plasma in K2EDTA (Innovative Research, USA) was centrifuged at 14 000 × *g* for 5 min and the supernatant was collected prior to loading into the size-exclusion column (iZON 70 nm pore size) for exosome isolation. For pre-clinical EV-chip validation studies, human plasma was obtained from young (n = 3; male; age range of 25–35 years) and old (n = 3; male; age range of 65–75 years) donors (BioIVT). Plasma samples from donors were de-identified however samples were controlled for gender, BMI, race, and ethnicity (Table 1, Supporting Information). Pre-clinical plasma samples were treated similarly to pooled plasma samples with exosome purification as previously described with the 70 nm pore size-exclusion column.

EV-Chip Surface Functionalization: 2-(*N*-Morpholino) ethane sulfonic acid (MES, Sigma) was prepared at 2×10^{-3} M at pH 6 and stored at room temperature. 1-Ethyl-3- [3-dimethylaminopropyl] carbodiimide hydrochloride (EDC) was supplied by G Biosciences. It was prepared at 200×10^{-3} M in MES 2×10^{-3} M, pH 6 immediately before using on the chip. *N*-Hydroxysuccinimide (NHS, Sigma, USA) was prepared at 400×10^{-3} M freshly and mixed with EDC at the same volume ratio immediately before using on the chip. PBA (Sigma, USA) was prepared at 750×10^{-3} M in dimethylformamide (DMF, Sigma, USA) and stored at room temperature and used for functionalization of graphene. Phosphate buffer saline (1× PBS, Gibco, USA) was diluted 1000-fold by adding 40 μL of 1× PBS to 40 mL of nuclease-free water.

Characterization of Exosomes: Exosomes were characterized using 1) size-based methods such as dynamic light scattering (DLS) and NTA, 2) protein quantification and characterization through Bradford assay and ELISA, and 3) morphology through scanning electron microscopy.

Dynamic Light Scattering: The size distribution and presence of exosomes of each fraction was measured with DLS (Malvern Panalytical). An amount of 50 µL of purified exosomes was loaded in a cuvette (ZEN0040, Malvern Panalytical) and the size distribution of particles was measured in the range of 40–150 nm. All pipet tips and cuvettes used for DLS measurements were washed three times with 0.22 µm filtered 1× PBS buffer to minimize particle contamination prior to introduction with exosome samples. DLS was only used as an indication that exosomes were present (or degraded) in samples prior to testing on EV-chip and that fraction diameters were consistent between experimental runs.

Nanoparticle Tracking Analysis: NTA is a very robust technique for quantification of total exosomes suspended in solution. When the sample is irradiated by a laser beam, scattered light signals from the Brownian motion of nanoparticles is collected by an optical microscope and complementary metal oxide semiconductor camera. An amount of 100 µL of purified exosomes was diluted 10-fold with 1× PBS for analysis. The concentration and particle size distribution of purified exosomes were quantified by NTA (Nanosight NS300, Malvern Panalytical) under optimal parameter settings at the Children's Hospital of Los Angeles, Extracellular Vesicle Core.

Total Protein Quantification Through Bradford Assay: Total protein concentration was quantified using a standard Bradford assay (Quick Start Kit, Bio-Rad) according to the manufacturer's instructions. In-short, 5 µL of exosome sample and 245 µL of dye reagent were incubated at 20 °C and analyzed with Nanodrop (Thermofisher) at an absorbance of 595 nm and compared to a BSA standard curve for confirmation of final protein quantification and sample purity.

ELISA Validation for CD63 Surface Protein Expression: Exosome surface marker characterization was defined with ExoELISA-Ultra CD63 Kit (System Biosciences, EXEL-ULTRA-CD63-1). Direct ELISA was performed according to the manufacturer's protocol. Briefly, exosome integrity was validated with DLS (average exosome diameter of 50.75 nm) and total protein content through Bradford assay (18.8 µg mL^{-1}) just prior to direct absorption of exosomes onto the kit provided Nunc Maxisorp 96-well plate. Subsequent primary and secondary antibody binding and detection through the enzymatic reaction of horse radish peroxidase (HRP) were carried out per the manufacturer's protocol. Absorbance of ExoELISA Ultra Super-sensitive TMB ELISA substrate was measured with a spectrophotometric plate reader at 450 nm. A standard ELISA calibration curve was established for correspondence to exosome sample concentration.

Scanning Electron Microscopy: SEM was incorporated to visually inspect the surface morphology of pristine graphene and exosome-immobilized gFETs. Before SEM characterization, each chip was dried with nitrogen gas and, subsequently, electroplated with 5 nm of pure gold to cover the entire gFET-exposed sample loading site. The gold coating preserves the exosomes for long-term storage and enhances electron conductivity for higher image quality. SEM was conducted at Pomona/Harvey Mudd College using Hitachi SU-70 Analytical UHR Schottky Emission Scanning Electron Microscope (Hitachi High-Tech Corporation, Tokyo, Japan) according to a standard protocol. In short, a voltage of 5.0 kV was applied, inducing an emission current of approximately 30 µA. Low magnification was set to observe the overall structure of gFETs while high magnification was employed when potential exosome binding sites were identified. Images on pristine graphene, e.g., graphene with nothing bound to it and exosome-immobilized gFETs were inspected collectively to better assess the distribution of antibodies as well as the morphology of exosomes.

Graphene Based Field-Effect Transistor: Fabrication and Reader Device: Graphene chips were designed and fabricated as previously described.[44,45] Each chip was fabricated in several steps using microelectromechanical systems processing.[41] Briefly, Ti/Pt source, drain, and reference electrodes with bond pads were patterned on 8′ silicon wafers using a lift-off processing technique. Wafers were then etched by piranha solution to remove organic contaminants that could act as dopants on the final graphene chips. Thereafter, a high-quality graphene layer was grown on a copper foil substrate and spin coated with a poly methyl methacrylate (PMMA). The gate voltage was swept between 0.1 and –0.1 V in a triangle wave at a slow speed of 0.3 Hz, while source-drain voltage (V_{SD}) was held at 50 mV for each transistor and capacitance response (C-response) was monitored in real-time. These voltage ranges were selected to minimize the electrical fields on exosome binding. The Agile Plus software (Cardea Bio, USA) was used to analyze the hardware responses. The effective surface potential (V-response) and U-response are also recorded in real-time. The collected responses were analyzed to assess exosome binding affinity. Data analysis was performed using Python scripts and Knime workflows to calculate capacitance and surface potential data. The averaged C-response for IgG and CD63 transistors was compared using Welch's *t*-test ($p < 0.01$).

Functionalization and Antibody Conjugation: Before functionalization of the graphene surface of EV-chip with a specific capture antibody, gFET chips were cleaned by rinsing with 30 µL of acetone followed by rinsing twice with 30 µL of nuclease-free water. The gFETs were then air-dried and subsequently functionalized with 15 µL of PBA (750×10^{-3} M, Sigma-Aldrich) in DMF for 1 h at room temperature. After the incubation, the

functionalized PBA chips were rinsed with 30 µL of DMF followed by two times rinsing with 30 µL of 70% ethanol and a single rinse with 30 µL of 100% isopropyl alcohol. PBA chips were then activated by a mixture of EDC (100×10^{-3} M) and NHS (200×10^{-3} M) in 2×10^{-3} M MES (pH 6.0) for 30 min at room temperature prior to incubation with CD63 capture antibody (Figure S2, Supporting Information). The excess amount of EDC/NHS was then washed four times with 2×10^{-3} M MES (pH 6). CD63 or CD151 antibodies (33.3 µg mL^{-1} in 1× PBS) were then immobilized atop the activated gFET surface for 30 min at room temperature. The unbound antibody was rinsed two times with 1× PBS (pH 7.4) and surface was blocked using bovine serum albumin (BSA) (166 µg mL^{-1} in 1× PBS) for 20 min at room temperature to minimize non-specific binding. After passivation with BSA, each chip was rinsed six times with 1/1000× PBS (pH 6.8) prior to calibration with real-time electrical measurement (Figure S2, Supporting Information).

Detection of Purified Exosomes on Antibody Functionalized gFET chip (EV-Chip): For each gFET chip, the gate voltage, V_G, was swept between −100 and +100 mV with a frequency of 3.3 Hz; supplied through the liquid-gate with a constant 100 mV source-drain voltage (V_{ds}). The source-drain current (I_{ds}) was measured for each V_G point and the average I_{ds} was recorded every 3.3 s. Each EV-chip was connected to the singleplex chip reader (Agile, Cardea Bio) for real-time detection at 37 °C. After functionalization with a specific antibody (CD63 or CD151), each EV-chip was passivated with BSA including a six times rinse with 1/1000× PBS (pH 6.8) as described previously. Each EV-chip was then calibrated with 1/1000× PBS (pH 6.8) for 5 min followed by sample introduction of the isolated exosomes in 1× PBS atop the chip for a 40-min incubation step at 37 °C. Afterwards, the surface was rinsed five times with 1/1000× PBS and an exosomal-binding response was measured after 16 min. A real-time electrical read-out in the form of either current (I-response), surface potential (V-response), or capacitance (C-response) was analyzed for statistical significance.

Statistical Analysis: Transistors exhibiting behavior indicative of electrical malfunction (current dropping to below 1 microamp) were excluded from consideration. For all other transistors, the real-time current readout (average I_{ds}) and capacitance or C-response were normalized by dividing by the I- or C-response immediately prior to the current assay step and multiplying by a scaling constant, while for voltage or V-response prior to the step was subtracted. The normalized I-, C-, and V-response at equilibrium (i.e., at the end of each assay step) were used as the measurement for that assay step.

Unless otherwise noted, the mean and standard error of the mean (SEM) are plotted, and all statistical tests were conducted using Prism v8. No transformations were applied, and no outliers were excluded. For the initial proof of concept, pooled plasma sample from healthy patients was assayed on anti-CD63- and anti-IgG1- (control) antibody functionalized chips with 15 replicates in each group. The C-response measurements on binding were normally distributed using the Shapiro–Wilk test ($p > 0.05$); consequently, the difference in means between CD63 and control was assessed using a two-tailed Welch's *t*-test (equal variance not assumed).

A standard curve was prepared using purified exosomes as described above with five replicate measurements per concentration. The curve was fit to a four-parameter logistic model using Prism v8. Subsequent experiments were conducted using three samples from young patients and three samples from old patients, with measurements performed on four chips with three transistors each for 12 measurements per patient. The protocol includes excluding any broken transistors from measurement and after excluding broken transistors, there were 34 measurements for anti-CD63, 32 measurements for anti-IgG, and 23 measurements for CD151 in each group, respectively. Each group was tested for normality using the Shapiro–Wilk test. Welch's two-tailed *t*-test was used to assess the difference in means for significance for the young versus old comparison and for all subsequent pairwise comparisons between the replicate measurements for two individuals from the two groups. Additionally, to classify young and old measurements, a LDA model was fit to the anti-CD151 data acquired for the young and old groups to find the threshold providing the best separation.

The averaged C-response for IgG and CD63 transistors was compared using Welch's *t*-test ($p < 0.01$).

Supporting Information

Supporting Information is available from the Wiley Online Library or from the author.

Acknowledgements

The authors acknowledge Dr. Paolo Neviani at the Children's Hospital Los Angeles for his contributions toward nanoparticle tracking analysis of exosome samples, Dr. Francie Barron, Ken Dickerson, and Daniel Levenson for their expertise on immunoassays, and Dr. Hsiang-Wei Lu for his consultation on the multiplexing potential of the device. This work was primarily supported by Cardea sponsored research to Aran lab, with support for J.J.T. from NSF INTERN award #1827671. Schematics in Figure 1, Figures S1 and S2 (Supporting Information) were created with BioRender.com.

Conflict of Interest

K.A. is a co-founder of Cardea.

Data Availability Statement

Data openly available in a public repository that issues datasets with DOIs 10.6084/m9.figshare.14099315.

Keywords

aging, biotechnology, exosomes, graphene, label-free, sensors, vesicles

Received: December 1, 2020
Revised: February 23, 2021
Published online:

[1] J. Kim, A. S. Campbell, B. E.-F. de Ávila, J. Wang, *Nat. Biotechnol.* **2019**, *37*, 389.
[2] Y. Bai, H. Zhao, *Ann. Transl. Med.* **2018**, *6*, S89.
[3] C. Franceschi, P. Garagnani, C. Morsiani, M. Conte, A. Santoro, A. Grignolio, D. Monti, M. Capri, S. Salvioli, *Front. Med.* **2018**, *5*, 61.
[4] E. Jaul, J. Barron, *Front. Public Health* **2017**, *5*, 335.
[5] B. Rj, B. Jm, W. Em, W. Kj, G. J, B. M, K. Ba, *Int. J. Alzheimer's Dis.* **2012**, *2012*, 903645.
[6] A. Bradford, M. E. Kunik, P. Schulz, S. P. Williams, H. Singh, *Alzheimer Dis. Assoc. Disord.* **2009**, *23*, 306.
[7] E. Eitan, J. Green, M. Bodogai, N. A. Mode, R. Bæk, M. M. Jørgensen, D. W. Freeman, K. W. Witwer, A. B. Zonderman, A. Biragyn, M. P. Mattson, N. Noren Hooten, M. K. Evans, *Sci. Rep.* **2017**, *7*, 1342.
[8] Alliance for Aging Research, https://www.agingresearch.org/health-topic/ (accessed: March 2021).
[9] M. Kankaanpää, M. Holma-Eriksson, S. Kapanen, M. Heitto, S. Bergström, L. Muukkonen, V.-P. Harjola, *BMC Emerg. Med.* **2018**, *18*, 43.

[10] T.-Y. Wei, Y. Fu, K.-H. Chang, K.-J. Lin, Y.-J. Lu, C.-M. Cheng, *Trends Biotechnol.* **2018**, *36*, 290.
[11] S. Nayak, N. R. Blumenfeld, T. Laksanasopin, S. K. Sia, *Anal. Chem.* **2017**, *89*, 102.
[12] A. Pfäfflin, E. Schleicher, *Anal. Bioanal. Chem.* **2009**, *393*, 1473.
[13] M. Agrawal, A. Biswas, *Front. Mol. Biosci.* **2015**, *2*, 54.
[14] G. Raposo, W. Stoorvogel, *J. Cell Biol.* **2013**, *200*, 373.
[15] M. Mitsuhashi, D. D. Taub, D. Kapogiannis, E. Eitan, L. Zukley, M. P. Mattson, L. Ferrucci, J. B. Schwartz, E. J. Goetzl, *FASEB J.* **2013**, *27*, 5141.
[16] K. Im, J. Baek, W. S. Kwon, S. Y. Rha, K. W. Hwang, U. Kim, H. Min, *Int. J. Gerontol.* **2018**, *12*, 233.
[17] G. G. de Andrade, L. R. Cechinel, K. Bertoldi, F. Galvão, P. V. Worm, I. R. Siqueira, *Neuroimmunomodulation* **2018**, *25*, 18.
[18] A. Gámez-Valero, J. Campdelacreu, D. Vilas, L. Ispierto, R. Reñé, R. Álvarez, M. P. Armengol, F. E. Borràs, K. Beyer, *Transl. Neurodegener.* **2019**, *8*, 31.
[19] E. J. Goetzl, M. Mustapic, D. Kapogiannis, E. Eitan, I. V. Lobach, L. Goetzl, J. B. Schwartz, B. L. Miller, *FASEB J.* **2016**, *30*, 3853.
[20] J. M. Silverman, D. Christy, C. C. Shyu, K.-M. Moon, S. Fernando, Z. Gidden, C. M. Cowan, Y. Ban, R. G. Stacey, L. I. Grad, L. McAlary, I. R. Mackenzie, L. J. Foster, N. R. Cashman, *J. Biol. Chem.* **2019**, *294*, 3744.
[21] Y. Wu, W. Deng, D. J. Klinke, *Analyst* **2015**, *140*, 6631.
[22] L. Barile, G. Vassalli, *Pharmacol. Ther.* **2017**, *174*, 63.
[23] R. Kalluri, V. S. LeBleu, *Science* **2020**, *367*, eaau6977.
[24] M. S. Pols, J. Klumperman, *Exp. Cell Res.* **2009**, *315*, 1584.
[25] N. Latysheva, G. Muratov, S. Rajesh, M. Padgett, N. A. Hotchin, M. Overduin, F. Berditchevski, *Mol. Cell. Biol.* **2006**, *26*, 7707.
[26] T. Lekishvili, E. Fromm, M. Mujoomdar, F. Berditchevski, *J. Cell Sci.* **2008**, *121*, 685.
[27] T. Yoshida, Y. Kawano, K. Sato, Y. Ando, J. Aoki, Y. Miura, J. Komano, Y. Tanaka, Y. Koyanagi, *Traffic* **2008**, *9*, 540.
[28] L. Källquist, M. Hansson, A.-M. Persson, H. Janssen, J. Calafat, H. Tapper, I. Olsson, *Blood* **2008**, *112*, 3444.
[29] S. N. Hurwitz, D. Nkosi, M. M. Conlon, S. B. York, X. Liu, D. C. Tremblay, D. G. Meckes, *J. Virol.* **2017**, *91*, e02251.
[30] Y. Jin, Y. Takeda, Y. Kondo, L. P. Tripathi, S. Kang, H. Takeshita, H. Kuhara, Y. Maeda, M. Higashiguchi, K. Miyake, O. Morimura, T. Koba, Y. Hayama, S. Koyama, K. Nakanishi, T. Iwasaki, S. Tetsumoto, K. Tsujino, M. Kuroyama, K. Iwahori, H. Hirata, T. Takimoto, M. Suzuki, I. Nagatomo, K. Sugimoto, Y. Fujii, H. Kida, K. Mizuguchi, M. Ito, T. Kijima, H. Rakugi, E. Mekada, I. Tachibana, A. Kumanogoh, *Sci. Rep.* **2018**, *8*, 5145.
[31] M. D'Anca, C. Fenoglio, M. Serpente, B. Arosio, M. Cesari, E. A. Scarpini, D. Galimberti, *Front. Aging Neurosci.* **2019**, *11*, 232.
[32] N. Noren Hooten, *Transl. Med. Aging* **2020**, *4*, 96.
[33] R. Sadej, A. Grudowska, L. Turczyk, R. Kordek, H. M. Romanska, *Lab. Invest.* **2014**, *94*, 41.
[34] X. A. Zhang, A. R. Kazarov, X. Yang, A. L. Bontrager, C. S. Stipp, M. E. Hemler, *Mol. Biol. Cell* **2002**, *13*, 1.
[35] U.S. Food & Drug Administration, https://www.fda.gov/news-events/press-announcements/fda-approves-first-liquid-biopsy-next-generation-sequencing-companion-diagnostic-test (accessed: August 2020).
[36] C. Alix-Panabières, *Nature* **2020**, *579*, S9.
[37] A. K. Mattox, C. Bettegowda, S. Zhou, N. Papadopoulos, K. W. Kinzler, B. Vogelstein, *Sci. Transl. Med.* **2019**, *11*, eaay1984.
[38] C. Rivet, H. Lee, A. Hirsch, S. Hamilton, H. Lu, *Chem. Eng. Sci.* **2011**, *66*, 1490.
[39] L. Nicu, T. Leïchlé, *J. Appl. Phys.* **2008**, *104*, 111101.
[40] Y. Yu, Y.-T. Li, D. Jin, F. Yang, D. Wu, M.-M. Xiao, H. Zhang, Z.-Y. Zhang, G.-J. Zhang, *Anal. Chem.* **2019**, *91*, 10679.
[41] S. Basu, P. Bhattacharyya, *Sensors and Actuators B: Chemical* **2012**, *173*, 1.
[42] G. Midekessa, K. Godakumara, J. Ord, J. Viil, F. Lättekivi, K. Dissanayake, S. Kopanchuk, A. Rinken, A. Andronowska, S. Bhattacharjee, T. Rinken, A. Fazeli, *ACS Omega* **2020**, *5*, 16701.
[43] A. N. Hoofnagle, M. H. Wener, *J. Immunol. Methods* **2009**, *347*, 3.
[44] R. Hajian, S. Balderston, T. Tran, T. deBoer, J. Etienne, M. Sandhu, N. A. Wauford, J.-Y. Chung, J. Nokes, M. Athaiya, J. Paredes, R. Peytavi, B. Goldsmith, N. Murthy, I. M. Conboy, K. Aran, *Nat. Biomed. Eng.* **2019**, *3*, 427.
[45] C. Sadlowski, S. Balderston, M. Sandhu, R. Hajian, C. Liu, T. P. Tran, M. J. Conboy, J. Paredes, N. Murthy, I. M. Conboy, K. Aran, *Lab Chip* **2018**, *18*, 3230.
[46] L. M. Silva, W. Wang, B. A. Allard, T. S. Pottorf, D. T. Jacobs, P. V. Tran, in *Methods in Cell Biology* (Ed.: T. Weimbs), Academic Press **2019**, pp. 205–229.
[47] S. Sharma, H. I. Rasool, V. Palanisamy, C. Mathisen, M. Schmidt, D. T. Wong, J. K. Gimzewski, *ACS Nano* **2010**, *4*, 1921.
[48] V. Sokolova, A.-K. Ludwig, S. Hornung, O. Rotan, P. A. Horn, M. Epple, B. Giebel, *Colloids Surf., B* **2011**, *87*, 146.
[49] C. Wiwie, J. Baumbach, R. Röttger, *Nat. Methods* **2015**, *12*, 1033.
[50] A. Shrivastava, V. B. Gupta, *Chron. Young Sci.* **2011**, *2*, 21.
[51] G. F. Reed, F. Lynn, B. D. Meade, *Clin. Diagn. Lab. Immunol.* **2002**, *9*, 1235.
[52] U.S. Food & Drug Administration, https://www.fda.gov/regulatory-information/search-fda-guidance-documents/bioanalytical-method-validation-guidance-industry (accessed: May 2020).
[53] R. Ekins, in *Immunoassays for the 80s* (Eds.: A. Voller, A. Bartlett, D. Bidwell), Springer, Netherlands, Dordrecht **1981**, pp. 5–16.
[54] Abnova, http://www.abnova.com/products/products_detail.asp?catalog_id=KA4926 (accessed: April 2021).
[55] System Biosciences, "ExoELISA-ULTRA Complete Kit (CD63 Detection) | System Biosciences," can be found under https://systembio.com/shop/exoelisa-ultra-complete-kit-cd63-detection/, (accessed: May 2020).
[56] HansaBioMed Life Sciences, https://galenlabsupplies.com/quantification-kits/ (accessed: April 2021).
[57] F. P. Schwarz, D. Tello, F. A. Goldbaum, R. A. Mariuzza, R. J. Poljak, *Eur. J. Biochem.* **1995**, *228*, 388.
[58] Immunochemistry Technologies, https://immunochemistry.com/educational-material/free-energy-basis-supporting-antibody-antigen-bond-formation/ (accessed: April 2021).
[59] H. Akiba, K. Tsumoto, *J. Biochem.* **2015**, *158*, 1.
[60] R. Perozzo, G. Folkers, L. Scapozza, *J. Recept. Signal Transduction Res.* **2004**, *24*, 1.
[61] D. Perez-Hernandez, C. Gutiérrez-Vázquez, I. Jorge, S. López-Martín, A. Ursa, F. Sánchez-Madrid, J. Vázquez, M. Yáñez-Mó, *J. Biol. Chem.* **2013**, *288*, 11649.
[62] ThermoFisher Scientific, "Is Your ELISA Kit Qualified and Validated?", https://www.thermofisher.com/blog/behindthebench/is-your-elisa-kit-qualified-and-validated/ (accessed: November 2020).
[63] Y. Bei, S. Das, R. S. Rodosthenous, P. Holvoet, M. Vanhaverbeke, M. C. Monteiro, V. V. S. Monteiro, J. Radosinska, M. Bartekova, F. Jansen, Q. Li, J. Rajasingh, J. Xiao, *Theranostics* **2017**, *7*, 4168.
[64] M. Medrano, L. Communal, K. R. Brown, M. Iwanicki, J. Normand, J. Paterson, F. Sircoulomb, P. Krzyzanowski, M. Novak, S. A. Doodnauth, F. S. Saiz, J. Cullis, R. Al-Awar, B. G. Neel, J. McPherson, R. Drapkin, L. Ailles, A.-M. Mes-Massons, R. Rottapel, *Cell Rep.* **2017**, *18*, 2343.
[65] E. van der Pol, A. N. Böing, P. Harrison, A. Sturk, R. Nieuwland, *Pharmacol. Rev.* **2012**, *64*, 676.